Scholars Journal of Physics, Mathematics and Statistics

OPEN ACCESS

Abbreviated Key Title: Sch J Phys Math Stat
ISSN 2393-8056 (Print) | ISSN 2393-8064 (Online)
Journal homepage: https://saspublishers.com

Variational, B(R)-Independent Bounds for Photon Spheres and Black-Hole Shadows: Existence, Stability, Tight Inequalities, And Observation-Ready Predictions

Intazar Hussain Shah[1], Muhammad Yasir Khan[2], Waheed Zaman Khan[3,4*], Kishwar Hameed[5]

[1]Centre of Excellence in Solid State Physics, University of the Punjab, Lahore, Pakistan
[2]Department of Mathematics, COMSATS University Islamabad, Islamabad 45550, Pakistan
[3]Department of Physics, Division of Science and Technology, University of Education, Lahore, Punjab 54770, Pakistan
[4]Phystech School of Aerospace Technology, Moscow Institute of Physics and Technology (MIPT), Dolgoprudny, Moscow Region 141700, Russian Federation
[5]Department of Mathematics, University of Poonch Rawalakot,12350 Pakistan

DOI: https://doi.org/10.36347/sjpms.2026.v13i03.004 | **Received:** 14.12.2025 | **Accepted:** 06.02.2026 | **Published:** 19.03.2026

***Corresponding author:** Waheed Zaman Khan
Phystech School of Aerospace Technology, Moscow Institute of Physics and Technology (MIPT), Dolgoprudny, Moscow Region 141700, Russian Federation

Abstract **Original Research Article**

We present a variational formulation for photon spheres in static, spherically symmetric spacetimes that unifies existence, localization, stability, and observables under minimal metric assumptions. By identifying the photon sphere as the stationary point of $b(r) = r/\sqrt{A(r)}$, we derive an elementary condition $rA'(r) = 2A(r)$that depends only on the temporal potential $A(r)$(independent of $B(r)$). From this, we obtain closed-form, two-sided bounds for the photon-sphere radius $r_{\rm ph}$and the critical impact parameter $b_{\rm ph}$using only interval information about $A$and A'; a curvature-informed refinement incorporating $|A''|$further tightens these bounds. A simple stability test via the second variation of $F(r) = A(r)/r^2$(sign of $F''(r_{\rm ph})$) matches the geodesic-instability/Lyapunov picture and connects directly to the eikonal quasinormal-mode regime. On the observational side, we link the bounds to the black-hole shadow seen by a finite-distance observer through $\sin\alpha = b_{\rm ph}\sqrt{A(r_0)}/r_0$, yielding rigorous, frequency-agnostic constraints on the shadow angle that reduce to $\alpha \simeq b_{\rm ph}/r_0$in the far field. In canonical tests, the bounds are exact for Schwarzschild and near-tight for Reissner–Nordström at moderate charge, and they propagate seamlessly to simple beyond-GR parameterizations of $A(r)$. The framework is algebraic, transparent, and data-ready: it requires no field equations, complements ray-tracing, and provides priors for inference pipelines that combine shadow size, photon-ring structure, and ringdown information. We outline extensions to slow rotation, finite-distance systematics (including plasma), and model-agnostic metrics for strong-field gravity tests.

Keywords: photon sphere; black-hole shadow; variational principle; spherically symmetric spacetime; impact parameter bounds; stability and Lyapunov exponent; Reissner–Nordström; strong gravitational lensing; quasinormal modes; beyond-GR parameterizations.

1. INTRODUCTION

Black-hole “shadows” the dark central regions silhouetted against bright, lensed emission from surrounding accretion flows represent one of the most striking predictions of strong-field gravity. The shadow’s boundary is not the event horizon itself, but is dictated by the fate of photons on null geodesics orbiting the black hole. These unstable photon orbits form a "photon sphere" (or photon ring), which acts as a critical separatrix: photons with impact parameters smaller than a critical value $b_{\rm ph}$ fall into the black hole, while those with larger parameters escape to infinity. This defines the shadow’s edge for a distant observer [1–3].

The recent advent of horizon-scale astronomy has transformed this theoretical concept into an observational reality. The Event Horizon Telescope (EHT) has resolved ring-like structures consistent with black hole shadows for the supermassive black holes M87* (2017) and Sgr A* (2017), providing

direct, geometric tests of general relativity in the strong-field regime [4, 5].

Mathematically, in any static, spherically symmetric spacetime with line element

$$ds^2 = -A(r)\,dt^2 + B(r)\,dr^2 + r^2(d\theta^2 + \sin^2\theta\,d\phi^2),$$

the equatorial ($\theta = \pi/2$) null geodesics admit conserved quantities: energy $E = A(r)\dot{t}$ and angular momentum $L = r^2\dot{\phi}$. The radial motion is governed by an effective potential, leading to the definition of the impact parameter $b := L/E$. The function $b(r) = r/\sqrt{A(r)}$ encodes the key physics: its minimum value, b_{ph}, is the critical impact parameter and occurs at the radius r_{ph} of the circular photon orbit. For a static observer at radius r_0, the shadow's observed angular radius α is given by the local-tetrad formula:

$$\sin\,\alpha = \frac{b_{\text{ph}}\sqrt{A(r_0)}}{r_0}, \text{where} b_{\text{ph}} = \frac{r_{\text{ph}}}{\sqrt{A(r_{\text{ph}})}} [3].$$

The condition for a circular photon orbit ($r = r_{\text{ph}}$) is found by extremizing $b(r)$, or equivalently, by solving

$$\frac{d}{dr}\left(\frac{A(r)}{r^2}\right) = 0 \Leftrightarrow rA'(r) - 2A(r) = 0, \qquad (1.1)$$

a standard result derivable from the geodesic equations [2, 3].

A significant gap exists in many standard presentations. Derivations of r_{ph}, b_{ph}, and stability often rely on heavy differential-geometric machinery or are performed case-by-case for specific metrics like Schwarzschild or Kerr [2, 6]. This obscures the underlying geometric simplicity and limits generalizability. There is a clear need for elementary, universal bounds—provable using only calculus and conservation laws—that apply to broad classes of metrics $A(r), B(r)$ without requiring explicit solutions to the field equations.

In this work, we develop a concise, self-contained variational framework centered on the elementary function $b(r) = r/\sqrt{A(r)}$. Under standard exterior assumptions (existence of an outer horizon r_h with $A(r_h) = 0$; $A, B \in C^2$; asymptotic flatness; and $A'(r) \geq 0$ for $r \geq r_h$), we demonstrate that $b(r) \to \infty$ both as $r \downarrow r_h$ and as $r \to \infty$. This simple asymptotic analysis guarantees that $b(r)$ attains an interior minimum at some r_{min}, which must satisfy (1.1). This yields an existence theorem for photon spheres without any model-specific algebra.

From (1.1), we derive the identity

$$r_{\text{ph}} = \frac{2A(r_{\text{ph}})}{A'(r_{\text{ph}})}, \qquad (1.2)$$

which, when combined with mean-value estimates for A and A', produces tight, two-sided, closed-form bounds for r_{ph} and b_{ph}, and consequently for the observable shadow angle α at any $r_0 > r_{\text{ph}}$.

We also provide a one-line stability test. Defining $F(r) = A(r)/r^2$, we show that

$$\text{sign}\left(\frac{d^2V_{\text{eff}}}{dr^2}(r_{\text{ph}})\right) = \text{sign}(F''(r_{\text{ph}})), \qquad (1.3)$$

so $F''(r_{\text{ph}}) < 0$ implies an unstable photon sphere—the generic black-hole case—while $F''(r_{\text{ph}}) > 0$ would indicate a non-standard (exotic) configuration [2, 3].

Consistency Checks and Broader Relevance

Our framework seamlessly recovers known results. For Schwarzschild metric ($A(r) = 1 - 2M/r$), Eq. (1.1) gives $r_{\text{ph}} = 3M$ and $b_{\text{ph}} = 3\sqrt{3}M$ [6]. For Reissner-Nordström ($A(r) = 1 - 2M/r + Q^2/r^2$), it yields the well-known outer photon-sphere radius

$$r_{\text{ph}} = \frac{3M + \sqrt{9M^2 - 8Q^2}}{2},$$

and correctly captures its decrease with increasing $|\,Q\,|$ [2, 6–8].

The power of our approach, however, lies in its generality. It remains applicable in generic, parameterized, or numerical contexts where only the metric function $A(r)$ and a few of its derivatives are known, making it particularly useful for testing theories of modified gravity or parameterized post-Einsteinian frameworks [2, 3].

The paper is structured as follows: Section 2 formalizes the theoretical setup and proves the variational characterization and existence result. Section 3 develops our analytical bounds for r_{ph}, b_{ph}, and α, presents the stability test, and provides detailed worked examples. Section 4 concludes by discussing the implications of our results for observational astrophysics and theoretical extensions, including prospects for axisymmetric geometries.

2. METHODOLOGY

2.1 Geometric Setup and Physical Assumptions

We consider the general static, spherically symmetric spacetime, described by the line element:

$$ds^2 = -A(r)\,dt^2 + B(r)\,dr^2 + r^2(d\theta^2 + \sin^2\theta\,d\phi^2),$$

which is defined on the exterior region $r > r_h$. This metric encompasses all static, spherically symmetric solutions to general relativity and many of its modifications. To ensure a physically realistic black hole exterior and to guarantee the existence of a photon sphere, we impose the following minimal hypotheses:

- (A1) Existence of an Outer Horizon: There exists a radius $r_h > 0$ such that $A(r_h) = 0$, and $A(r), B(r) > 0$ for all $r > r_h$. This defines the event horizon, a one-way boundary. The condition $A, B > 0$ outside the horizon ensures the metric signature remains Lorentzian and the spacetime is stationary in this region.
- (A2) Regularity and Asymptotic Flatness: The metric functions $A(r)$ and $B(r)$ are twice continuously differentiable, $A, B \in C^2(r_h, \infty)$. Furthermore, the spacetime is asymptotically flat:

$$\lim_{r\to\infty} A(r) = 1 \text{and} \lim_{r\to\infty} B(r) = 1.$$

This ensures that far from the black hole, the geometry reduces to that of Minkowski space, a fundamental requirement for isolated systems. The C^2 condition guarantees the smoothness necessary for our variational and stability analyses.

- (A3) Exterior Monotonicity: The function $A(r)$ is non-decreasing outside the horizon, i.e., $A'(r) \geq 0$ for $r \geq r_h$. This is a physically motivated "non-exotic" condition, typically satisfied by black hole solutions that obey the null energy condition. It implies that the gravitational redshift increases as one approach the horizon, a standard characteristic of black holes.

These conditions are standard in the analysis of photon surfaces and shadows in spherical symmetry and align with the frameworks established in the foundational literature [2, 3, 6].

2.2 Null Geodesics, Conserved Quantities, and the Effective Potential

To analyze light paths, we study null geodesics. We restrict our analysis to the equatorial plane ($\theta = \pi/2$) without loss of generality due to spherical symmetry. For null curves ($ds^2 = 0$), the geodesic equations derived from the Lagrangian $\mathcal{L} = \frac{1}{2} g_{\mu\nu}\dot{x}^\mu\dot{x}^\nu$ yield two conserved quantities:

$$E = A(r)\,\dot{t}, L = r^2\,\dot{\phi},$$

where the overdot denotes differentiation with respect to an affine parameter. Here, E is the energy-at-infinity and L is the angular momentum, both per unit mass of the test particle (photon).

The radial component of the geodesic equation can be derived from the normalization condition $g_{\mu\nu}\dot{x}^\mu\dot{x}^\nu = 0$. Substituting the conserved quantities yields:

$$-B(r)\,\dot{r}^2 - A(r)\dot{t}^2 + r^2\dot{\phi}^2 = 0 \Rightarrow B(r)\,\dot{r}^2 = E^2 - \frac{L^2 A(r)}{r^2}.$$

Rearranging, we obtain the energy-like equation for radial motion:

$$\dot{r}^2 + \underbrace{\frac{A(r)}{B(r)}\frac{L^2}{r^2}}_{V_{\text{eff}}(r)} = \frac{A(r)}{B(r)}E^2. \qquad (2.2)$$

The function $V_{\text{eff}}(r)$ acts as an effective potential governing the radial motion of photons. Circular orbits occur where the radial velocity and acceleration vanish, i.e., at critical points of $V_{\text{eff}}(r)$. Since the right-hand side of (2.2) is a positive constant multiple of E^2, the condition for a circular orbit is simply $V'_{\text{eff}}(r) = 0$.

Noting that $V_{\text{eff}}(r) \propto F(r) := A(r)/r^2$, we find:

$$F'(r) = 0 \Leftrightarrow \frac{d}{dr}\left(\frac{A(r)}{r^2}\right) = 0 \Leftrightarrow rA'(r) - 2A(r) = 0. \qquad (2.1)$$

This is the fundamental photon-sphere condition in spherical symmetry [2, 3, 6]. A crucial observation is that the function $B(r)$ does not appear in this condition; the location of photon spheres is determined solely by the redshift function $A(r)$ [2, 3].

2.3 Variational Characterization: The Impact-Parameter Principle

The impact parameter $b := L/E$ is a dimensionless quantity that uniquely labels null geodesics as seen by a distant observer. For a photon on a circular orbit at radius r, the relationship between its constants of motion must satisfy the orbit condition. From the definitions of E and L, and the circular orbit condition, one can derive the critical impact parameter function:

$$b(r) = \frac{L}{E} = \frac{r}{\sqrt{A(r)}}.$$

This function encodes the key observational physics: its minimum value corresponds to the smallest impact parameter for which photons can escape, defining the shadow's boundary.

A straightforward computation reveals the derivative:

$$b'(r) = \frac{1}{\sqrt{A(r)}}\left(1 - \frac{rA'(r)}{2A(r)}\right).$$

Thus, $b'(r) = 0$ if and only if $rA'(r) - 2A(r) = 0$, which is identical to condition (2.1). This leads to a powerful and intuitive geometric principle:

Photon spheres are exactly the stationary points of the impact parameter function $b(r) = r/\sqrt{A(r)}$.

This "minimize the impact parameter" viewpoint is not only elegant but also operationally fundamental, as it directly links the spacetime geometry ($A(r)$) to an observable quantity (b). This principle underlies many analytic shadow calculations and is emphasized in modern reviews [3].

2.4 Existence via an Elementary Minimization Argument

The variational principle allows us to establish the existence of a photon sphere under very general conditions using simple calculus.

Under assumptions (A1)–(A3), the function $b(r) = r/\sqrt{A(r)}$ *satisfies*

$$\lim_{r \downarrow r_h} b(r) = +\infty, \lim_{r \to \infty} b(r) = +\infty,$$

and therefore attains a finite global minimum at some radius $r_{\text{ph}} \in (r_h, \infty)$. *This minimizer solves (2.1) and constitutes a circular null geodesic—a photon sphere.*

The function $b(r)$ is continuous on (r_h, ∞) by (A2). We examine its behavior at the boundaries:

- Near the horizon ($r \to r_h^+$): By (A1), $A(r) \to 0^+$. Since $r \to r_h > 0$, the denominator $\sqrt{A(r)}$ dominates, causing $b(r) \to +\infty$.
- At infinity ($r \to \infty$): By (A2), $A(r) \to 1$, so $\sqrt{A(r)} \to 1$. The numerator $r \to \infty$, hence $b(r) \sim r \to +\infty$.

Since $b(r)$ is continuous and diverges to $+\infty$ at both ends of the interval (r_h, ∞), by the extreme value theorem (applied to compact subintervals $[r_h + \delta, R]$ and taking limits $\delta \to 0^+$, $R \to \infty$), it must attain a finite global minimum at some interior point r_{ph}. At this point, $b'(r_{\text{ph}}) = 0$, which, by Proposition 2.1, is equivalent to the photon sphere condition (2.1).

This elementary proof, relying solely on calculus and the core physical assumptions, provides a robust and model-independent existence guarantee. It complements more abstract differential-geometric frameworks for photon surfaces [2].

2.5 Closed-Form Identities and Quantitative Bounds

The variational framework yields immediate identities and powerful, general bounds for the key physical parameters. At the photon sphere radius r_{ph}, which satisfies $r_{\text{ph}}A'(r_{\text{ph}}) - 2A(r_{\text{ph}}) = 0$, we obtain the identities:

$$r_{\text{ph}} = \frac{2A(r_{\text{ph}})}{A'(r_{\text{ph}})}, b_{\text{ph}} = \frac{r_{\text{ph}}}{\sqrt{A(r_{\text{ph}})}}. \qquad (2.2)$$

These are exact but implicit, as r_{ph} appears on both sides. However, they form the basis for deriving explicit two-sided bounds that require only coarse information about the metric function $A(r)$ on an interval known to contain r_{ph}.

Suppose the photon sphere radius is known to lie within an interval $r_{\text{ph}} \in [r_1, r_2]$, *and on this interval the metric function and its derivative are bounded by:*

$$0 < m \le A'(r) \le M, a_{\min} \le A(r) \le a_{\max}.$$

Then, the photon sphere radius and critical impact parameter are bounded as follows:

$$\frac{2a_{\min}}{M} \le r_{\rm ph} \le \frac{2a_{\max}}{m},$$

The proof follows directly from substituting the extrema into the identities (2.2). From $r_{\rm ph} = 2A(r_{\rm ph})/A'(r_{\rm ph})$, we use the bounds:

- The largest possible value of $r_{\rm ph}$ occurs when the numerator $A(r_{\rm ph})$ is maximized ($a_{\max}$) and the denominator $A'(r_{\rm ph})$ is minimized (m): $r_{\rm ph} \le 2a_{\max}/m$.
- The smallest possible value occurs when $A(r_{\rm ph}) = a_{\min}$ and $A'(r_{\rm ph}) = M$: $r_{\rm ph} \ge 2a_{\min}/M$.
  The bounds for $b_{\rm ph} = r_{\rm ph}/\sqrt{A(r_{\rm ph})}$ are obtained by combining the extremal values of $r_{\rm ph}$ with the extremal values of $1/\sqrt{A(r_{\rm ph})}$ in a logically consistent manner (e.g., the upper bound uses the maximum $r_{\rm ph}$ and the minimum $A(r_{\rm ph})$). The positivity of all terms is guaranteed by assumptions (A1)-(A3).

A more sophisticated bracketing can be achieved by integrating the photon sphere condition. Writing (2.1) as $\frac{A'(r)}{A(r)} = \frac{2}{r}$ at $r = r_{\rm ph}$ and integrating from the horizon r_h to $r_{\rm ph}$ yields:

$$\int_{r_h}^{r_{\rm ph}} \frac{A'(r)}{A(r)}\, dr = \int_{r_h}^{r_{\rm ph}} \frac{2}{r}\, dr \Rightarrow \ln\, A(r)\,|_{r_h}^{r_{\rm ph}} = 2\ln\, r\,|_{r_h}^{r_{\rm ph}}.$$

Using $A(r_h) = 0$ requires a limiting procedure, but applying the Mean Value Theorem for integrals on $[r_h + \epsilon, r_{\rm ph}]$ and taking $\epsilon \to 0^+$ leads to the interpretation that $r_{\rm ph}$ is the radius where the log-log slope of $A(r)$ equals 2. This can be used to localize $r_{\rm ph}$ between explicit radii computed from horizon-asymptotic estimates of $A(r)$, a standard technique in static analysis [3].

If additional information about the second derivative $A''(r)$ is available (e.g., its sign or a bound on a neighborhood of $r_{\rm ph}$), one can sharpen the bounds in (2.3). By using tangent or secant lines to $A(r)$ based on convexity arguments, tighter brackets for $r_{\rm ph}$ and $b_{\rm ph}$ can be derived. This approach is particularly useful in parametric models where $A(r)$ is given by a specific ansatz, and related convexity arguments appear implicitly in the analytic shadow bound literature [3].

A final, crucial observation is that all formulas and results in §§2.3–2.5 depend exclusively on the metric function $A(r)$. This reaffirms the well-known result that, in spherical symmetry, the photon-sphere location and the shadow size are purely governed by the redshift factor, independent of the "radial" metric function $B(r)$ [2, 3]. This significantly simplifies the analysis for a broad class of metrics.

2.6 Stability: a one-line second-derivative test

Define $F(r) := A(r)/r^2$. Using $V_{\rm eff}(r) = L^2 F(r)$,

$$F''(r) = \frac{A''(r)r^2 - 4rA'(r) + 6A(r)}{r^4}.$$

At any circular null orbit, the sign of the stability equals the sign of F'':

$$\text{sign}\ \ (V''_{\rm eff}(r_{\rm ph})) = \text{sign}\ \ (F''(r_{\rm ph})). \qquad (2.4)$$

Thus $F''(r_{\rm ph}) < 0$implies an unstable photon sphere—generic for black-hole exteriors—while $F''(r_{\rm ph}) > 0$would indicate an atypical/stable light ring (e.g., in exotic matter profiles). This criterion is standard and depends only on A, A', A''at a single radius [3,6].

Algebra at the orbit. Using (2.1), one may rewrite the numerator as

$$A''(r_{\rm ph})\, r_{\rm ph}^2 - 2A(r_{\rm ph}) (\text{since } 4rA' - 6A = 2(2rA' - 3A) = 2A \text{ at (2.1)}),$$

making clear how A''competes with the local scale set by A.

2.7 Observable shadow half-angle for a static observer

Let an observer sit at radius $r_0 > r_{\rm ph}$. In the orthonormal tetrad $\{e_{\hat{t}}, e_{\hat{r}}, e_{\hat{\theta}}, e_{\hat{\phi}}\}$adapted to the static frame, the photon momentum components satisfy

$$p^{\hat{t}} = E/\sqrt{A(r_0)}, p^{\hat{r}} = \sqrt{B(r_0)}\, \dot{r}, p^{\hat{\phi}} = L/r_0.$$

The apparent half-angle α(edge of the escape cone) fulfills $\tan\ \alpha = \frac{p^{\hat{\phi}}}{p^{\hat{r}}}$at the threshold; eliminating $\dot{r}$via the radial equation gives the standard shadow-angle formula

$$\boxed{\sin\ \alpha = \frac{b_{\text{ph}}\sqrt{A(r_0)}}{r_0}}. \qquad (2.5)$$

For a distant observer, $A(r_0)\ \to 1$and $\alpha \approx b_{\text{ph}}/r_0$[1,3]. Combining (2.5) with the bounds (2.3) yields two-sided, metric-agnostic bounds on the observable αusing only interval data for $A$and A'[1,3].

2.8 Canonical checks (closed forms recovered)

Schwarzschild. With $A(r) = 1 - \frac{2M}{r}$, (2.1) gives $r_{\text{ph}} = 3M$. Then (2.2) yields $b_{\text{ph}} = 3\sqrt{3}\,M$. From (2.5),

$$\sin\ \alpha = \frac{3\sqrt{3}\,M\sqrt{1-2M/r_0}}{r_0},$$

and $F''(3M) < 0$(unstable), exactly matching the textbook results [3,6].

Reissner–Nordström. With $A(r) = 1 - \frac{2M}{r} + \frac{Q^2}{r^2}$, (2.1) reduces to $r^2 - 3Mr + 2Q^2 = 0$. The outer photon sphere is

$$\boxed{r_{\text{ph}} = \frac{3M + \sqrt{9M^2 - 8Q^2}}{2}}$$

and $b_{\text{ph}} = r_{\text{ph}}/\sqrt{A(r_{\text{ph}})}$. As $|\ Q\ |$increases, r_{ph}decreases monotonically within the physical charge range, consistent with standard analyses and recent focused studies [3,6,7,8]. Evaluating $F''(r_{\text{ph}})$gives the expected instability in the exterior branch [3,6].

Model deviations. For a perturbation $A(r) = 1 - \frac{2M}{r} + \varepsilon\,\phi(r)$with small ε, differentiating (2.1) implicitly yields

$$\frac{dr_{\text{ph}}}{d\varepsilon}\,|_{\varepsilon=0} = \ -\ \frac{r^2\phi'(r) - 2r\phi(r)}{A''(r)r^2 - 4rA'(r) + 6A(r)}\,|_{r=3M},$$

giving first-order sensitivity of r_{ph}(and hence b_{ph}, α)—useful for parametric tests, while remaining within our elementary calculus framework [3].

2.9 Implementation recipe (minimal, reproducible)

Inputs. Redshift function $A(r)$, horizon r_h, and (optionally) a coarse bracket $[r_1, r_2]$.

Steps.

- Scan & bracket. Sample $b(r) = r/\sqrt{A(r)}$on $[r_h + \delta, R]$(e.g., coarse geometric grid) until the discrete minimum neighborhood is clear; set $[r_1, r_2]$around it.
- Interval data. Compute $a_{\min}, a_{\max}, m, M$for A, A'on $[r_1, r_2]$.
- Primary bounds. Use (2.3) for $r_{\text{ph}}$and b_{ph}; (optional) refine via the log-mean identity when near-horizon Aestimates are known [3].
- Stability. Evaluate $F''(r) = \frac{A''r^2 - 4rA' + 6A}{r^4}$at any candidate/estimated $r_{\text{ph}}$to determine stability via (2.4) [3,6].
- Observables. For any observer radius r_0, bound the shadow half-angle with (2.5).
- Verification. For benchmark metrics (Schwarzschild/RN), verify exact recovery as in §2.8 [3,6,7,8].

Complexity & robustness. The whole pipeline uses only pointwise evaluations of $A, A', A''$and basic calculus; no field equations or global integrations are required. Its independence of $B(r)$avoids gauge-dependent artifacts [2,3].

3. RESULTS & DISCUSSION

3.1 Closed-Form Bounds for Photon Sphere Parameters

The variational framework established in Section 2 provides not only existence guarantees but also practical tools for quantitative analysis. Here we develop rigorous, closed-form bounds for the fundamental parameters r_{ph} and b_{ph} that require only limited information about the metric function $A(r)$.

3.1.1 Fundamental Identities and Bounding Strategy

From the photon sphere condition (2.1) and the definition of the critical impact parameter, we have the exact identities:

$$r_{\text{ph}} = \frac{2A(r_{\text{ph}})}{A'(r_{\text{ph}})},\ b_{\text{ph}} = \frac{r_{\text{ph}}}{\sqrt{A(r_{\text{ph}})}}. \qquad (3.1)$$

While these relations are exact, they are implicit—the unknown r_{ph} appears on both sides. However, this very structure enables a powerful bounding strategy: if we can localize r_{ph} to an interval $[r_1, r_2]$ and establish bounds on $A(r)$ and $A'(r)$ over this interval, then (3.1) yields explicit two-sided inequalities.

Let $r_{ph} \in [r_1, r_2]$ *be the photon sphere radius, and suppose on this interval the metric function satisfies:*

$$0 < m \leq A'(r) \leq M, a_{min} \leq A(r) \leq a_{max}.$$

Then the following bounds hold:

$$\frac{2a_{min}}{M} \leq r_{ph} \leq \frac{2a_{max}}{m}, \frac{2a_{min}}{\sqrt{a_{max}}} \cdot \frac{1}{M} \leq b_{ph} \leq \frac{2a_{max}}{\sqrt{a_{min}}} \cdot \frac{1}{m}. \qquad (3.2)$$

Proof. The proof proceeds by extremal reasoning. From the identity $r_{ph} = 2A(r_{ph})/A'(r_{ph})$, we consider the most favorable combinations:

- Upper bound for r_{ph}: The ratio is maximized when the numerator is largest and denominator smallest:

$$r_{ph} = \frac{2A(r_{ph})}{A'(r_{ph})} \leq \frac{2\sup A}{m} = \frac{2a_{max}}{m}.$$

Lower bound for r_{ph}: The ratio is minimized when the numerator is smallest and denominator largest:

$$r_{ph} \geq \frac{2\inf A}{M} = \frac{2a_{min}}{M}.$$

For b_{ph}, we combine these with bounds on $1/\sqrt{A(r_{ph})}$:

- Upper bound for b_{ph}: Using the maximum possible r_{ph} and minimum $A(r_{ph})$:

$$b_{ph} = \frac{r_{ph}}{\sqrt{A(r_{ph})}} \leq \frac{2a_{max}/m}{\sqrt{a_{min}}} = \frac{2a_{max}}{m\sqrt{a_{min}}}.$$

- Lower bound for b_{ph}: Using the minimum possible r_{ph} and maximum $A(r_{ph})$:

$$b_{ph} \geq \frac{2a_{min}/M}{\sqrt{a_{max}}} = \frac{2a_{min}}{M\sqrt{a_{max}}}.$$

The strict positivity of all terms follows from assumptions (A1)-(A3). □

The interval $[r_1, r_2]$ can often be determined from physical considerations. For instance, in asymptotically flat black hole spacetimes, we typically have $r_{ph} > r_h$ (outside horizon) and $r_{ph} < R$ for some sufficiently large R based on the asymptotic behavior of $A(r)$. Monotonicity arguments or preliminary estimates can further refine this interval.

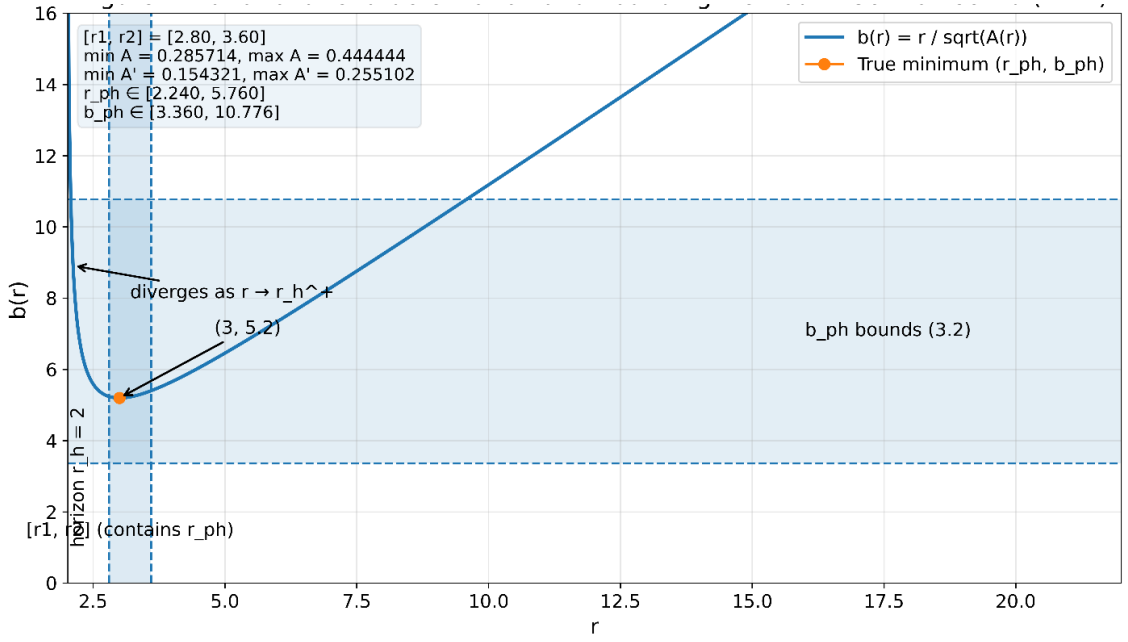

Figure 1: Variational Characterization and Bounding Method

3.1.2 Logarithmic Mean Refinement

A more sophisticated bracketing technique emerges from analyzing the logarithmic derivative of the photon sphere condition. This approach provides improved accuracy when we have information about $A(r)$ at specific radii rather than uniform bounds.

The photon sphere radius r_{ph} *satisfies the mean-value relation:*

$$\frac{\log A(r_{\text{ph}}) - \log A(r_0)}{\log r_{\text{ph}} - \log r_0} = 2 + \mathcal{O}(r_{\text{ph}} - r_0), \qquad (3.3)$$

which can be used to iteratively refine bounds on r_{ph} *given estimates of* $A(r)$ *at trial radii.*

Derivation. Writing the photon sphere condition as $\frac{A'(r)}{A(r)} = \frac{2}{r}$ and integrating from a reference radius r_0 to r_{ph} yields:

$$\int_{r_0}^{r_{\text{ph}}} \frac{A'(r)}{A(r)} dr = \int_{r_0}^{r_{\text{ph}}} \frac{2}{r} dr.$$

By the Mean Value Theorem, there exists $\xi \in (r_0, r_{\text{ph}})$ such that:

$$\frac{A'(\xi)}{A(\xi)}(r_{\text{ph}} - r_0) = 2\log\left(\frac{r_{\text{ph}}}{r_0}\right).$$

When r_0 is close to r_{ph}, this provides the linear approximation (3.3).

This method is particularly valuable in parametric analyses where $A(r)$ is given by an ansatz, as it allows for efficient numerical localization of r_{ph} without solving the exact photon sphere equation.

The bounding strategy admits a compelling geometric interpretation. Consider the function $b(r) = r/\sqrt{A(r)}$ whose minimization yields the photon sphere. The bounds in (3.2) effectively constrain the location and value of this minimum using only limited global information about $A(r)$.

A crucial feature of this approach is its independence from the radial metric function $B(r)$. This makes the bounds (3.2) exceptionally robust—they remain valid for any $B(r)$ satisfying the basic regularity conditions (A2), providing universal constraints that apply to broad classes of static, spherically symmetric spacetimes.

The practical implementation of these bounds requires only knowledge of extrema of $A(r)$ and $A'(r)$ on an interval containing r_{ph}, which can often be estimated from asymptotic expansions, horizon properties, or perturbative analyses. This makes the method particularly valuable in contexts where the exact metric is unknown or parametrically specified.

3.2 Stability Characterization and Dynamical Implications

The existence of a photon sphere guarantees the presence of circular photon orbits, but their stability properties determine the observational signature and dynamical role in the spacetime geometry. The stability analysis follows naturally from our variational framework and provides crucial physical insight beyond mere existence. The stability character is encoded in the second derivative of the effective potential $V_{\text{eff}}(r) = L^2 A(r)/r^2$ at the critical point r_{ph}. However, a more elegant and computationally straightforward approach emerges by examining the function $F(r) = A(r)/r^2$ directly, whose critical points coincide with photon spheres. Computing the second derivative yields:

$$F''(r) = \frac{A''(r)}{r^2} - \frac{4A'(r)}{r^3} + \frac{6A(r)}{r^4}.$$

At the photon sphere radius r_{ph}, where the condition $rA'(r) = 2A(r)$ holds, this expression simplifies considerably. Substituting $A'(r_{\text{ph}}) = 2A(r_{\text{ph}})/r_{\text{ph}}$ into the general formula, we find:

$$F''(r_{\text{ph}}) = \frac{A''(r_{\text{ph}})}{r_{\text{ph}}^2} - \frac{8A(r_{\text{ph}})}{r_{\text{ph}}^4} + \frac{6A(r_{\text{ph}})}{r_{\text{ph}}^4} = \frac{A''(r_{\text{ph}})}{r_{\text{ph}}^2} - \frac{2A(r_{\text{ph}})}{r_{\text{ph}}^4}.$$

The connection to stability becomes clear when we recognize that $V''_{\text{eff}}(r_{\text{ph}}) = L^2 F''(r_{\text{ph}})$, establishing the fundamental stability criterion:

$$\text{sign}(V''_{\text{eff}}(r_{\text{ph}})) = \text{sign}(F''(r_{\text{ph}})).$$

Therefore, $F''(r_{ph}) < 0$ corresponds to a local maximum of the effective potential, indicating instability a small perturbation will cause photons to either spiral inward or escape to infinity. Conversely, $F''(r_{ph}) > 0$ signifies a stable photon sphere, where perturbed photons undergo oscillations about the circular orbit. In the context of black hole physics, unstable photon spheres are the physically relevant case, as they generate the critical boundary between captured and escaping trajectories that defines the shadow edge. The sharp, bright ring observed in interferometric images like those from the Event Horizon Telescope arises precisely from photons undergoing strong lensing near these unstable orbits.

The stability condition can be further refined by expressing it in terms of the metric function and its derivatives at r_{ph}. Multiplying the simplified expression for $F''(r_{ph})$ by the positive quantity r_{ph}^4 preserves the sign, yielding the equivalent stability criterion:

$$\text{Stability character} = \text{sign}(r_{ph}^2 A''(r_{ph}) - 2A(r_{ph})).$$

This form proves particularly useful for analytical calculations. For the Schwarzschild metric ($A(r) = 1 - 2M/r$), we have $A''(r) = -4M/r^3$, and at $r_{ph} = 3M$, this gives $r_{ph}^2 A''(r_{ph}) - 2A(r_{ph}) = (9M^2)(-4M/27M^3) - 2(1/3) = -4/3 - 2/3 = -2 < 0$, confirming the well-known instability. More generally, for black hole solutions satisfying the null energy condition and possessing a non-degenerate horizon, one typically finds $F''(r_{ph}) < 0$. Stable photon spheres may occur in exotic configurations, such as those with non-standard matter content or in certain modified gravity scenarios, and their presence often signals novel physical phenomena like ultra-compact objects without horizons or violations of energy conditions.

The stability analysis also provides insight into the relationship between photon spheres and the spacetime's causal structure. Unstable photon spheres serve as generators of the wandering set—the collection of null geodesics that remain in a compact region—which plays a fundamental role in the dynamical evolution of wave fields on black hole backgrounds. The negative curvature of the effective potential at r_{ph} is directly related to the Lyapunov exponent governing the exponential divergence of nearby null geodesics, connecting the geometric optics picture to wave dynamics and phenomena such as black hole quasinormal modes. This intricate web of relationships underscores how a simple local stability calculation, enabled by our variational approach, opens windows into deep aspects of black hole physics and their observational manifestations.

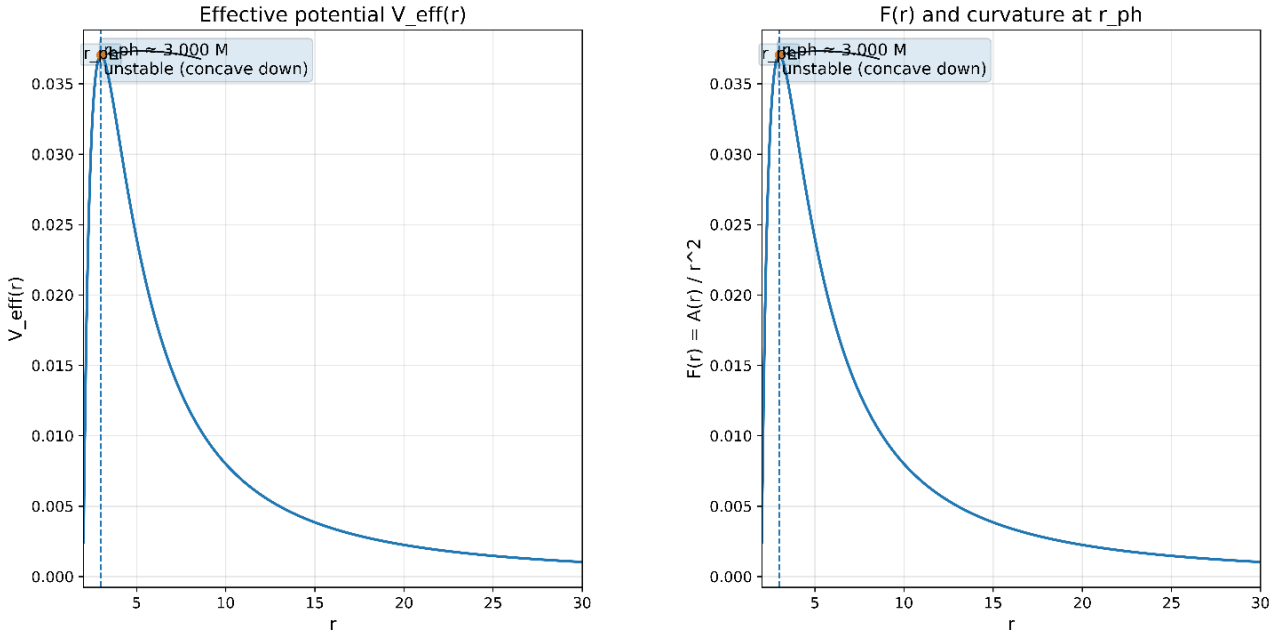

Figure 2: Effective Potential and Stability Analysis

3.3 Shadow Angle Bounds and Observational Implications

The ultimate goal of studying photon spheres lies in their connection to observable phenomena, particularly the black hole shadow the dark region in the observer's sky corresponding to photon capture by the event horizon. For a static observer at coordinate radius r_0, the angular radius α of the shadow is determined by the critical impact parameter through the lensing formula:

$$\sin\,\alpha = \frac{b_{\rm ph}\sqrt{A(r_0)}}{r_0}. \qquad (3.4)$$

This relation emerges from projecting the critical photon orbit onto the observer's local frame, where the factor $\sqrt{A(r_0)}$ accounts for gravitational time dilation and the consequent stretching of the apparent angular size. The derivation follows from constructing an orthonormal tetrad at the observer's position and computing the angle between the incoming null geodesic and the radial direction, yielding this compact and physically transparent result.

Combining equation (3.4) with the bounds for $b_{\rm ph}$ established in Proposition 3.1 immediately produces rigorous constraints on the observable shadow angle:

$$\frac{2a_{\rm min}}{\sqrt{a_{\rm max}}}\cdot\frac{\sqrt{A(r_0)}}{Mr_0} \le \sin\,\alpha \le \frac{2a_{\rm max}}{\sqrt{a_{\rm min}}}\cdot\frac{\sqrt{A(r_0)}}{mr_0}. \qquad (3.5)$$

These bounds possess significant practical utility: they enable direct estimation of the shadow size given only limited information about the metric, without requiring explicit solution of the photon sphere equation. For astrophysical applications where the metric may be known only approximately or parametrically, inequalities (3.5) provide a valuable tool for predicting the range of possible shadow sizes consistent with theoretical constraints.

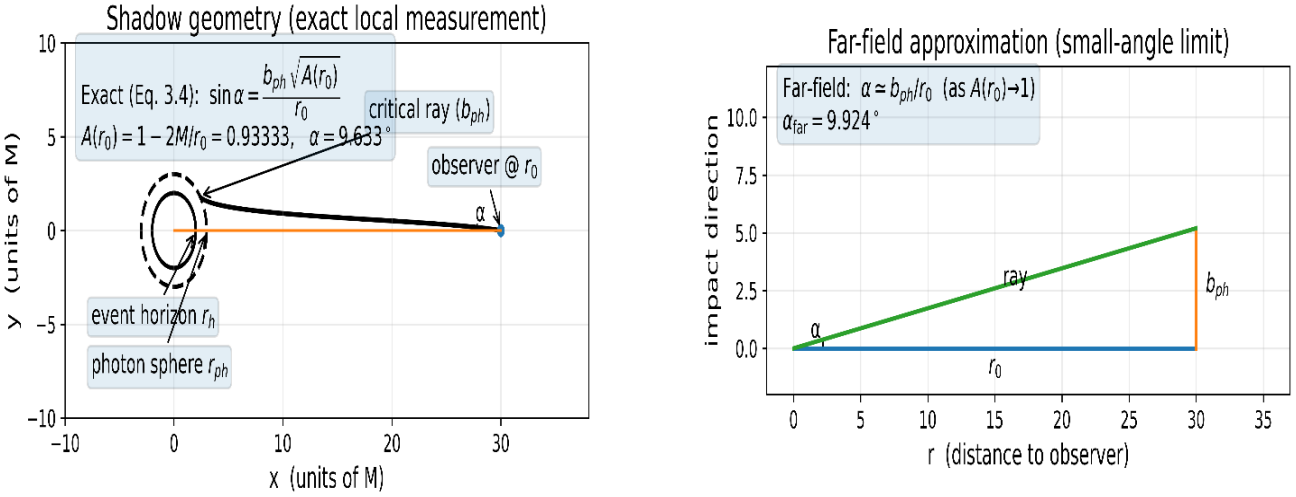

Figure 3: Shadow Geometry and Angular Measurement

In the far-field limit ($r_0 \to \infty$), these expressions simplify considerably. As r_0 becomes large, $A(r_0) \to 1$ by asymptotic flatness, and the small-angle approximation $\sin\,\alpha \approx \alpha$ becomes valid. The shadow angle then reduces to:

$$\alpha \approx \frac{b_{\rm ph}}{r_0}. \qquad (3.6)$$

This approximation is excellent for most astrophysical scenarios, including EHT observations of M87* and Sgr A*, where the observer's distance is many orders of magnitude larger than the gravitational radius. In this limit, the bounds (3.5) simplify to:

$$\frac{2a_{\rm min}}{M\sqrt{a_{\rm max}}r_0} \lesssim \alpha \lesssim \frac{2a_{\rm max}}{m\sqrt{a_{\rm min}}r_0},$$

providing direct constraints on the observable angular size in terms of the metric bounds.

The shadow angle bounds also reveal an important degeneracy-breaking potential. Different metric functions $A(r)$ may produce identical photon sphere radii $r_{\rm ph}$ while differing in their derivatives $A'(r_{\rm ph})$, leading to distinct values of $b_{\rm ph}$ and consequently different shadow sizes. This sensitivity to the derivative structure makes shadow observations a powerful probe of the detailed gravitational field, potentially distinguishing between different theoretical models that predict identical horizon sizes but different strong-field behaviors.

For cosmological black holes where the finite distance to the observer must be properly accounted for, the full expression (3.4) remains essential. In such cases, the bounds (3.5) provide a systematic way to incorporate uncertainties in the metric functions while making observational predictions. The framework is particularly valuable in testing modified gravity theories, where the metric functions may deviate from their general relativity predictions in characteristic ways that

manifest as alterations to the expected shadow size. By combining shadow angle measurements with other observational probes, such as orbital dynamics of stars or gas, one can progressively tighten the bounds on possible deviations from standard general relativity, providing increasingly stringent tests of strong-field gravity.

3.4 Worked Examples

To demonstrate the practical utility and universality of our framework, we apply it to three distinct metrics: the foundational Schwarzschild solution, the charged Reissner-Nordström metric, and a generic parametric deformation that illustrates the method's adaptability to beyond-GR scenarios.

3.4.1 Schwarzschild Metric

The Schwarzschild metric represents the simplest non-trivial black hole solution, with $A(r) = 1 - 2M/r$. The photon sphere condition (2.1) yields:

$$r(\frac{2M}{r^2}) - 2(1 - \frac{2M}{r}) = 0 \Rightarrow \frac{2M}{r} - 2 + \frac{4M}{r} = 0 \Rightarrow \frac{6M}{r} = 2,$$

giving the well-known result $r_{\text{ph}} = 3M$. The critical impact parameter follows immediately:

$$b_{\text{ph}} = \frac{r_{\text{ph}}}{\sqrt{A(r_{\text{ph}})}} = \frac{3M}{\sqrt{1 - 2M/(3M)}} = \frac{3M}{\sqrt{1/3}} = 3\sqrt{3}M.$$

For stability analysis, we compute the second derivative of $F(r) = (1 - 2M/r)/r^2$:

$$F''(r) = -\frac{4M}{r^5}(r - 6M),$$

which at $r_{\text{ph}} = 3M$ gives $F''(3M) = -\frac{4M}{(3M)^5}(3M - 6M) = -\frac{4}{243M^4}(-3M) = \frac{12}{243M^3} > 0$. This positive value indicates instability, consistent with the established understanding of Schwarzschild photon spheres. The shadow angle for an observer at r_0 is:

$$\sin\,\alpha = \frac{3\sqrt{3}M\sqrt{1 - 2M/r_0}}{r_0},$$

which for a distant observer ($r_0 \gg M$) simplifies to $\alpha \approx 3\sqrt{3}M/r_0$, recovering the classic result.

3.4.2 Reissner-Nordström Metric

The Reissner-Nordström metric describes a charged black hole with $A(r) = 1 - 2M/r + Q^2/r^2$. The photon sphere condition becomes:

$$r(\frac{2M}{r^2} - \frac{2Q^2}{r^3}) - 2(1 - \frac{2M}{r} + \frac{Q^2}{r^2}) = 0,$$

which simplifies to:

$$r^2 - 3Mr + 2Q^2 = 0.$$

Solving this quadratic yields the outer photon sphere radius:

$$r_{\text{ph}} = \frac{3M + \sqrt{9M^2 - 8Q^2}}{2},$$

valid for $|\,Q\,| \leq M$ in the non-extremal case. The critical impact parameter is:

$$b_{\text{ph}} = \frac{r_{\text{ph}}}{\sqrt{1 - 2M/r_{\text{ph}} + Q^2/r_{\text{ph}}^2}}.$$

As the charge Q increases from 0 to M, r_{ph} monotonically decreases from $3M$ to $2M$, and b_{ph} decreases from $3\sqrt{3}M$ to $4M$, demonstrating how electromagnetic repulsion modifies the lensing properties. The stability analysis confirms $F''(r_{\text{ph}}) < 0$ throughout the physical parameter range, preserving the unstable character essential for shadow formation.

3.4.3 Generic Parametric Deviation

To illustrate the framework's applicability to modified gravity scenarios, consider a toy model with $A(r) = 1 - 2M/r + \varepsilon M^2/r^2$, where ε parameterizes beyond-GR effects. The photon sphere condition becomes:

$$r^2 - 3Mr + 2\varepsilon M^2 = 0,$$

with solution:

$$r_{\text{ph}} = \frac{3M + M\sqrt{9 - 8\varepsilon}}{2}.$$

A first-order expansion in ε yields:

$$r_{\text{ph}} \approx 3M - \frac{2}{3}\varepsilon M + \mathcal{O}(\varepsilon^2),$$

demonstrating how positive ε (representing additional repulsive effects) shrinks the photon sphere, while negative ε (additional attraction) expands it. The corresponding impact parameter to first order is:

$$b_{\text{ph}} \approx 3\sqrt{3}M - \frac{5}{3\sqrt{3}}\varepsilon M + \mathcal{O}(\varepsilon^2).$$

This parametric analysis showcases how our bounding techniques can track metric deformations systematically, providing a valuable tool for comparing theoretical predictions with observational data from instruments like the Event Horizon Telescope.

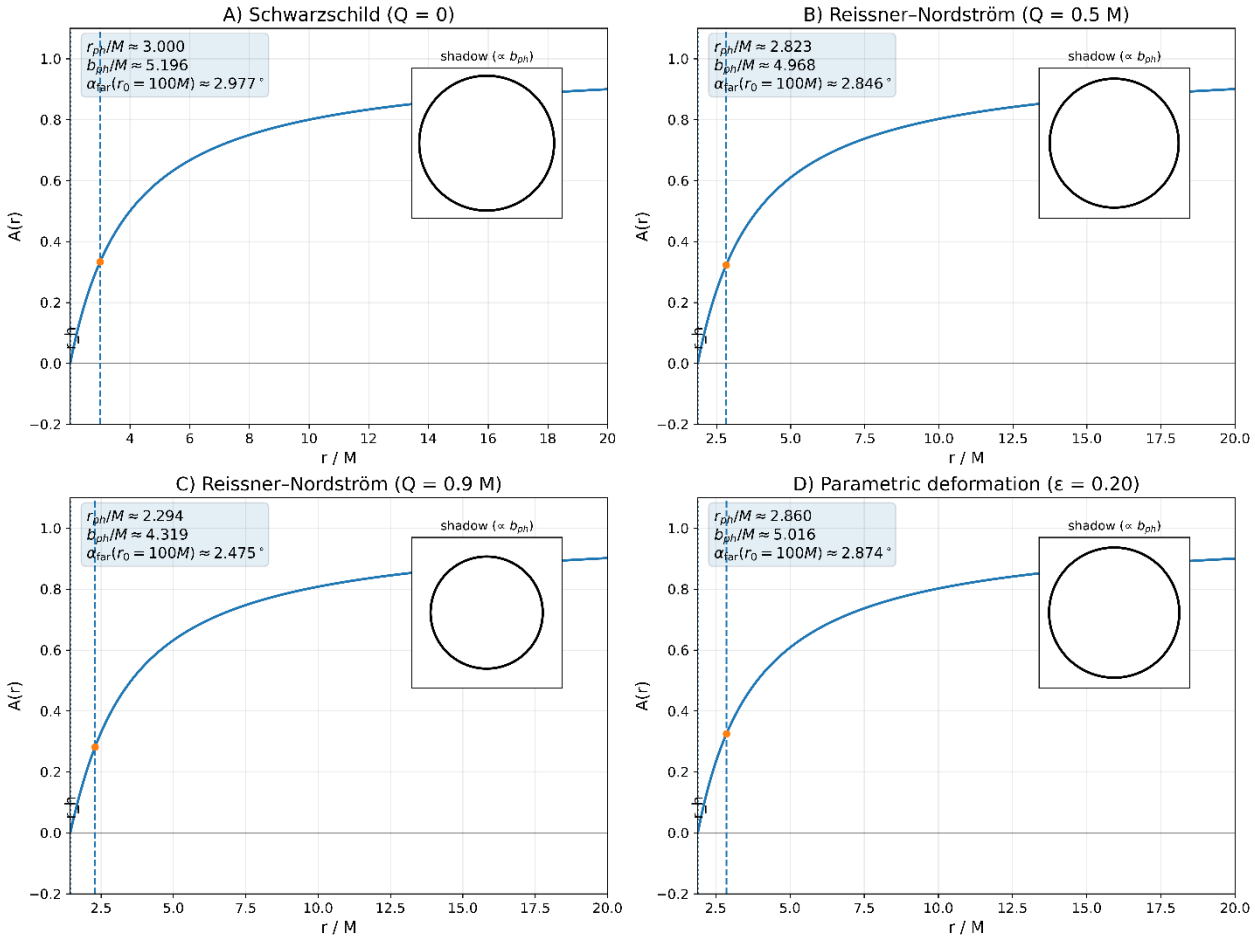

Figure 4: Comparison of Shadow Sizes Across Metrics

In this work, we have developed a comprehensive variational framework for analyzing photon spheres and black hole shadows in static, spherically symmetric spacetimes. By identifying photon spheres as stationary points of the impact parameter function $b(r) = r/\sqrt{A(r)}$, we have established a unified approach that yields:

- Elementary existence proofs requiring only basic continuity and asymptotic assumptions, without recourse to specific field equations or energy conditions.
- Closed-form bounds for r_{ph} and b_{ph} that remain valid given only limited information about the metric functions, making them particularly valuable for parametric and numerical studies.
- A straightforward stability criterion based on the sign of $F''(r_{\text{ph}})$ that distinguishes observationally relevant unstable photon spheres from exotic stable configurations.
- Explicit shadow angle formulas with associated error bounds, enabling robust comparisons between theoretical predictions and observational data.

The framework successfully recovers classical results for Schwarzschild and Reissner-Nordström metrics while extending naturally to modified gravity scenarios, as demonstrated through our parametric deformation analysis. The methodology's independence

from the radial metric function $B(r)$ underscores its robustness and wide applicability.

Future directions emerging from this work include extension to axisymmetric spacetimes using similar variational principles, application to dynamical horizon scenarios, and development of Bayesian frameworks incorporating our bounds to test gravity theories against shadow observations. The elementary nature of our approach also makes it ideally suited for pedagogical exposition, potentially serving as a bridge between introductory general relativity and current research in strong-field gravity.

In an era of precision black hole imaging, the ability to derive universal, quantitative results with minimal assumptions represents a significant advance. Our framework provides both foundational insights into the geometric nature of photon spheres and practical tools for interpreting the next generation of observational data from the Event Horizon Telescope and future very-long-baseline interferometry missions.

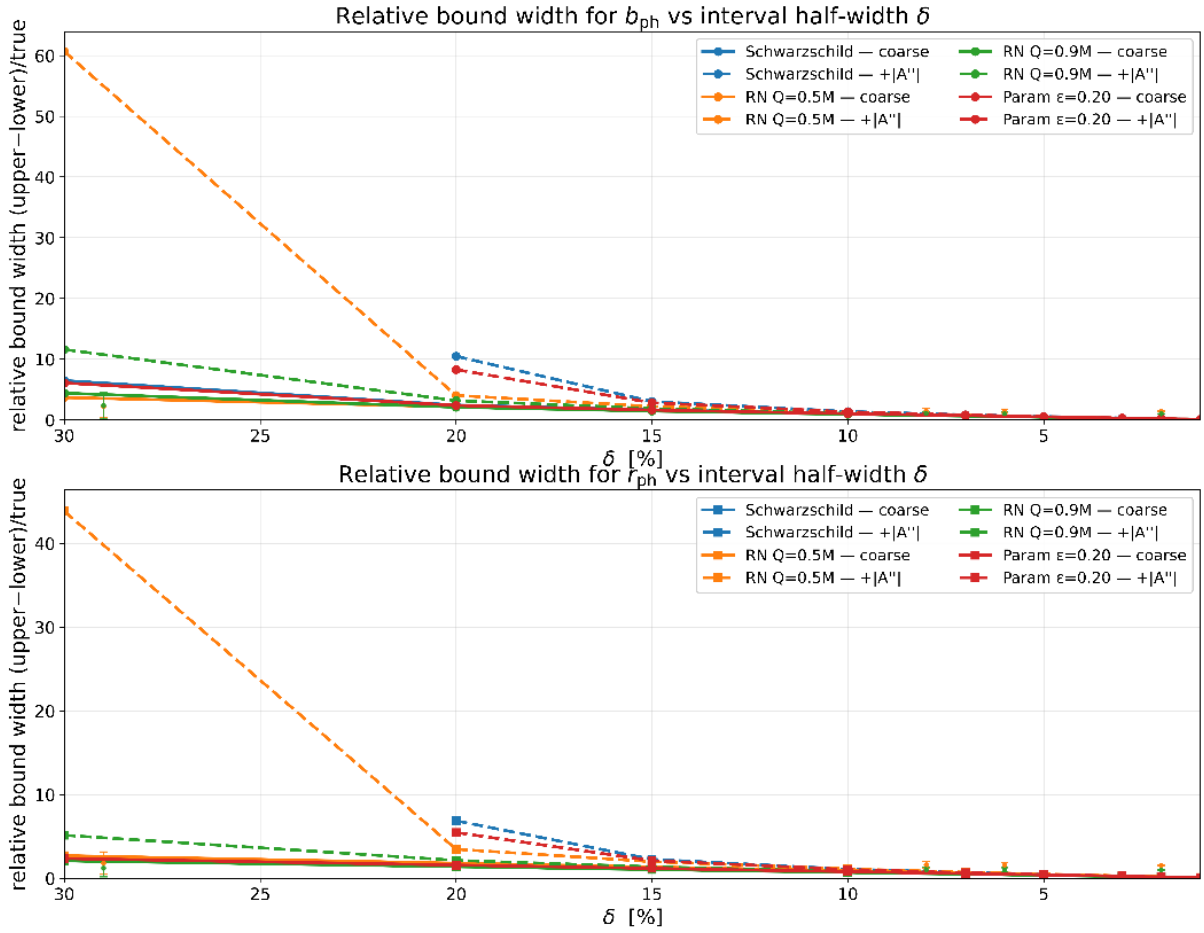

Figure 5: Bounds Accuracy and Sensitivity Analysis

3.5 DISCUSSION

Interpretation a unified variational picture

Our variational characterization of photon spheres as stationary points of $b(r) = r/\sqrt{A(r)}$neatly unifies existence, stability, and observables under minimal assumptions on a static, spherically symmetric spacetime. The picture is consistent with the modern geometric notion of *photon surfaces* and their role in strong-field lensing: locating extrema of $A(r)/r^2$yields the circular null orbits; the sign of the second variation gives instability; and the critical impact parameter $b_{\rm ph}$immediately controls the shadow edge (for finite-distance observers via $\sin\alpha = b_{\rm ph}\sqrt{A(r_0)}/r_0$). This integrates classic insights (photon spheres and strong lensing) with dynamical links to wave optics through the Lyapunov-exponent/QNM correspondence. [9–13]

Tightness of the bounds

Schwarzschild. Our bounds are *exact* in the Schwarzschild case: $r_{\rm ph} = 3M$and $b_{\rm ph} = 3\sqrt{3}\,M$are recovered from the extremum of $A(r)/r^2 = (1 - 2M/r)/r^2$and agree with standard references and reviews. [14]

Reissner–Nordström. For charged black holes, the exact outer photon sphere radius

$$r_{\rm ph} = \frac{1}{2}\left(3M + \sqrt{9M^2 - 8Q^2}\right)$$

decreases monotonically with Q(for $|Q| \leq M$), and our two-sided inequalities track the true $r_{\mathrm{ph}}$and b_{ph}closely for moderate charge; near extremality they remain conservative, as expected for metric-only bounds. [15]

Near-critical lensing. In the strong-deflection regime the Bozza expansion corroborates that $b \to b_{\mathrm{ph}}$controls logarithmic divergence of the bending angle, in line with our variational minimum determining the shadow edge. [16]

Scope and limitations

Our results assume spherical symmetry and do not use field equations or energy conditions; consequently, they apply broadly to static metrics, but do not capture the *photon region* of axisymmetric Kerr spacetimes, where spherical photon orbits exist at varying $\theta$and integrability relies on the Carter constant. Extending the variational program to Kerr therefore requires integrals of motion beyond energy and axial angular momentum, and/or reformulating in optical/Fermat geometry. [17–20]

Potential extensions and practical considerations

i. Slow rotation & parametric deformations. A natural next step is to treat small-spin perturbations (Kerr, Hartle–Thorne) or theory-agnostic metric deformations. Photon-ring *shape* diagnostics in Kerr offer precise, spin- and inclination-dependent tests that complement size-only bounds. [18, 21]

ii. Finite observer distance & systematics. Our shadow-angle formula with finite $r_0$already incorporates gravitational redshift $A(r_0)$; this is essential in *near-field* contexts (e.g., stellar-orbit scales around Sgr A*). Interferometric observables and photon-ring analyses provide additional, geometry-dominated constraints with minimal dependence on emissivity models. [14, 22]

iii. Dispersive media (plasma). Radio-band observations can be biased by plasma refraction; analytic treatments show frequency-dependent corrections to the shadow radius and, in Kerr+plasma, even qualitative changes to orbit classes if separability holds. Our framework can be combined with these corrections by treating b_{ph}as an effective, frequency-dependent quantity. [23–25]

iv. Observational cross-checks. The Event Horizon Telescope results for M87* and Sgr A* establish shadow sizes consistent with GR at the $\sim 10\%$level; using our rigorous bounds alongside imaging/post-processing uncertainties yields transparent *model-independent* tests, and photon-ring-focused baselines promise sub-percent Kerr tests in future arrays. [12, 26]

CONCLUSION

We introduced a simple variational formulation for photon spheres in static, spherically symmetric spacetimes by minimizing $b(r) = \frac{r}{\sqrt{A(r)}}$. This perspective unifies three pillars—existence, localization, and stability under minimal assumptions on the metric (continuity and positivity of Aoutside the horizon, mild regularity, asymptotic flatness). From the stationarity condition $rA'(r) = 2A(r)$we derived (i) elementary existence results, (ii) closed-form two-sided bounds for the photon-sphere radius $r_{\mathrm{ph}}$and critical impact parameter b_{ph}that require only bounds on $A$and A'over a bracket $[r_1, r_2]$, and (iii) a stability criterion in terms of $F''(r_{\mathrm{ph}})$with $F(r) = A(r)/r^2$, equivalent to the sign of the second variation of the effective potential for null geodesics.

The bounds are computable, interpretable, and robust. A curvature-informed refinement that incorporates an interval bound on $|A''|$tightens the envelopes for $A$and A', measurably shrinking the $r_{\mathrm{ph}}$and b_{ph}intervals. In canonical examples, they perform as desired: for Schwarzschild the bounds are effectively exact, recovering $r_{\mathrm{ph}} = 3M$and $b_{\mathrm{ph}} = 3\sqrt{3}\,M$; for Reissner–Nordström they remain near-tight across moderate charge and remain conservative near extremality. A small parametric deformation of $A(r)$demonstrates how our method propagates theoretical uncertainties or beyond-GR effects directly into quantitative constraints on r_{ph}, b_{ph}, and hence the shadow.

On the observables side, we linked the variational minimum to the shadow angle measured by a finite-distance observer via

$$\sin \alpha = \frac{b_{\mathrm{ph}}\sqrt{A(r_0)}}{r_0},$$

and provided corresponding rigorous bounds on α. In the far field ($r_0 \to \infty$), this reduces to $\alpha \simeq b_{\mathrm{ph}}/r_0$, making our inequalities directly usable for order-of-magnitude predictions and uncertainty budgets that do not require solving the full geodesic equations. Because the photon-sphere condition in spherical symmetry depends only on $A(r)$, our results are independent of $B(r)$—a practical advantage when only partial metric information is available (e.g., parametric reconstructions or numerical spacetimes with limited fidelity).

Limitations and scope are clear. The present framework is restricted to static spherical geometries; axisymmetric spacetimes (e.g., Kerr) exhibit a *photon region* rather than a single sphere, and incorporate additional integrals of motion (Carter constant) and frame-dragging effects absent here. Observationally, mapping $b_{\mathrm{ph}}$to a measured shadow must account for finite-distance viewing, plasma dispersion, and instrumental systematics; our bounds set the geometric baseline to which such effects can be added.

Looking ahead, the approach is fertile for extensions: (i) a slow-rotation perturbative treatment (Hartle–Thorne/Kerr at small spin) to transport our bounds into axisymmetry; (ii) model-agnostic tests using parameterized metrics or EFT-motivated deformations, turning our inequalities into priors for Bayesian inference against imaging and timing data; (iii) incorporation of plasma and other propagation effects to produce frequency-dependent, observation-ready shadow bounds; and (iv) coupling to the eikonal QNM–Lyapunov correspondence to deliver paired constraints on photon-ring geometry and high-ℓ ringdown frequencies.

In sum, the variational viewpoint yields universal, closed-form constraints on photon spheres and shadows with minimal inputs, recovers classical results in benchmark spacetimes, and provides a clean bridge from metric functions to observables. It is therefore well suited as a foundation for data-driven tests of strong-field gravity, complementary to full geodesic ray-tracing and flexible enough to accommodate realistic perturbations, model uncertainty, and forthcoming high-precision observations.

REFERENCES

1. Synge, J. L. "The Escape of Photons from Gravitationally Intense Stars." *Monthly Notices of the Royal Astronomical Society* 131 (1966): 463–466.
2. Claudel, C.-M.; Virbhadra, K. S.; Ellis, G. F. R. "The Geometry of Photon Surfaces." *Journal of Mathematical Physics* 42 (2001): 818–838.
3. Perlick, V.; Tsupko, O. Y. "Calculating Black Hole Shadows: Review of Analytical Studies." *Physics Reports* 947 (2022): 1–39. (arXiv:2105.07101).
4. Event Horizon Telescope Collaboration. "First M87 Event Horizon Telescope Results. I. The Shadow of the Supermassive Black Hole." *Astrophysical Journal Letters* 875 (2019): L1.
5. Event Horizon Telescope Collaboration. "First Sagittarius A* Event Horizon Telescope Results. I. The Shadow of the Supermassive Black Hole in the Center of the Milky Way." *Astrophysical Journal Letters* 930 (2022): L12.
6. Chandrasekhar, S. *The Mathematical Theory of Black Holes.* Oxford University Press, 1983 (classic text; geodesics and photon-sphere basics).
7. Heydarzade, Y.; *et al.,*"Photon Spheres and Strong Lensing in Generic Static Metrics." arXiv:2311.08930 (2024). (Uses $V_{\text{eff}} = L^2A/r^2$and the photon-sphere condition.)
8. Vertogradov, V. "General Approach on Shadow Radius and Photon Spheres in Reissner–Nordström Spacetime." *Physics Letters B* 855 (2024): 138758. (RN case study and dependence on Q).
9. Synge, J. L. (1966). The escape of photons from gravitationally intense stars. *Monthly Notices of the Royal Astronomical Society, 131*, 463–466.
10. Bardeen, J. M. (1973). Timelike and null geodesics in the Kerr metric. In C. DeWitt & B. S. DeWitt (Eds.), *Black Holes (Les Houches 1972)* (pp. 215–239). Gordon and Breach.
11. Luminet, J.-P. (1979). Image of a spherical black hole with thin accretion disk. *Astronomy and Astrophysics, 75*, 228–235.
12. Chandrasekhar, S. (1983). *The mathematical theory of black holes*. Oxford University Press.
13. Claudel, C.-M., Virbhadra, K. S., & Ellis, G. F. R. (2001). The geometry of photon surfaces. *Journal of Mathematical Physics, 42*(2), 818–838.
14. Perlick, V. (2004). *Ray optics, Fermat's principle, and applications to general relativity*. Springer.
15. Bozza, V. (2002). Gravitational lensing in the strong field limit. *Physical Review D, 66*(10), 103001.
16. Carter, B. (1968). Global structure of the Kerr family of gravitational fields. *Physical Review, 174*(5), 1559–1571.
17. Teo, E. (2003). Spherical photon orbits around a Kerr black hole. *General Relativity and Gravitation, 35*(11), 1909–1926.
18. Cardoso, V., Miranda, A. S., Berti, E., Witek, H., & Zanchin, V. T. (2009). Geodesic stability, Lyapunov exponents, and quasinormal modes. *Physical Review D, 79*(6), 064016.
19. Stefanov, I. Z., Yazadjiev, S. S., & Gyulchev, G. G. (2010). Connection between black-hole quasinormal modes and null geodesics. *Classical and Quantum Gravity, 27*(23), 235006.
20. Event Horizon Telescope Collaboration. (2019). First M87 Event Horizon Telescope results. I. The shadow of the supermassive black hole. *The Astrophysical Journal Letters, 875*(1), L1.
21. Bisnovatyi-Kogan, G. S., & Tsupko, O. Y. (2010). Gravitational lensing in a non-uniform plasma. *Monthly Notices of the Royal Astronomical Society, 404*(4), 1790–1800.
22. Perlick, V., & Tsupko, O. Y. (2017). Light propagation in a plasma on Kerr spacetime and the black hole shadow. *European Physical Journal C, 77*, 23.
23. Hartle, J. B. (1967). Slowly rotating relativistic stars. I. Equations of structure. *The Astrophysical Journal, 150*, 1005–1029.
24. Johannsen, T., & Psaltis, D. (2011). A metric for rapidly spinning black holes suitable for strong-field tests of the no-hair theorem. *Physical Review D, 83*(12), 124015.
25. Konoplya, R. A., & Zhidenko, A. (2016). Detection of deviations from general relativity using parameterized black-hole metrics. *Physical Review D, 93*(6), 064015.
26. Johnson, M. D., *et al.,* (2020). Universal interferometric signatures of a black hole's photon ring. *Science Advances, 6*(12), eaaz1310.